Evolution of the structural and microstructural characteristics of SrSn$_{1-x}$Ti$_x$O$_3$ thin films under the influence of the composition, the substrate and the deposition method

André Luiz Menezes de Oliveira [a,b,*], Valérie Bouquet [a], Vincent Dorcet [a], Sophie Ollivier [a], Stéphanie Députier [a], Antônio Gouveia de Souza [b], Maximo Siu-Li [c], Elson Longo [d], Ingrid Távora Weber [e], Iêda Maria Garcia dos Santos [b], Maryline Guilloux-Viry [a]

[a] Institut des Sciences Chimiques de Rennes, UMR 6226 CNRS/Université de Rennes 1, Campus de Beaulieu, 35042 Rennes Cedex, France
[b] LACOM/INCTMN, DQ, Universidade Federal de Paraiba, Campus I, CEP 58059-900 João Pessoa, PB, Brazil
[c] IFSC, Universidade de São Paulo, CEP 13560-970 São Carlos, SP, Brazil
[d] LIEC/CDMF, Instituto de Química, UNESP, P.O. Box 355, CEP 14801-970 Araraquara, SP, Brazil
[e] LIMA, Instituto de Química, Universidade de Brasília, CEP 70910-900 Brasília, DF, Brazil

ARTICLE INFO

ABSTRACT

SrSn$_{1-x}$Ti$_x$O$_3$ thin films were grown on R-sapphire and (100) LaAlO$_3$ single crystal substrates by two different routes: chemical solution deposition (CSD) and pulsed laser deposition (PLD). Structural and microstructural characteristics of the films were determined by X-ray diffraction (θ–2θ, ω- and φ-scans) and field emission scanning electron microscopy. Pure perovskite phase was obtained for all of the compositions, whatever the method of deposition and the substrate nature. On R-sapphire, a randomly oriented growth (polycrystalline) was observed for all of the compositions deposited by CSD while (h00) preferential orientation was attained when deposition was done by PLD, in particular for SrTiO$_3$ composition. The phi-scan performed on this sample revealed that the (100) oriented grains present an in-plane ordering (epitaxial growth) with respect to the substrate with an alignment of the [011] direction of the film along the [12$\bar{1}$] direction of the substrate, explained on the basis of misfit considerations and interface arrangements. All of the films grown on (100) LaAlO$_3$ exhibited an epitaxial growth with an in-plane relationship ⟨010⟩$_{film}$ // ⟨010⟩$_{substrate}$. As for the thin film microstructure, porosity, homogeneity, shape and size of the grains were strongly influenced by Ti content in the SrSn$_{1-x}$Ti$_x$O$_3$ solid solution, and also by the nature of the substrate and by the deposition method. Moreover, the influence of the composition and thin film growth on the photoluminescence of SST films were also evaluated.

© 2017 Elsevier B.V. All rights reserved.

1. Introduction

Strontium titanate SrTiO$_3$ with cubic structure (space group $Pm\bar{3}m$ [1]) is one of the most popular perovskite being used in different applications such as dynamic random access memories [2], tunable microwave devices [3], oxygen-gas sensors [4] and photocatalysts [5]. On the other hand, strontium stannate SrSnO$_3$ is a perovskite which presents an orthorhombic structure (space group $Pbnm$ [6]) with a great potential for a variety of technological applications, such as capacitors [7], insulating layer for high-temperature superconductor single-flux-quantum circuits [8], lithium-ion batteries [9], photocatalysts [10] and humidity sensors [11].

Alkaline-earth titanates stannates have also been studied in their combined forms A(Ti,Sn)O$_3$ (A = Ca, Sr and/or Ba). Barium titanate stannate solid solution Ba(Ti$_{1-x}$Sn$_x$)O$_3$ has been the most investigated one since the discovery of the strong broadening of ferroelectric phase transitions [12–15]. This solid solution has been widely studied in bulk [16,17], thin films [18,19] and thick films forms [20], correlating the Ti substitution with its properties. In contrast, the Sr(Sn,Ti)O$_3$ solid solution has not been as much investigated. Wu et al. [21] have reported the synthesis of strontium titanate stannate Sr(Sn,Ti)O$_3$ ceramics by solid state reaction and observed that SrSn$_{0.50}$Ti$_{0.50}$O$_3$ is a promising humidity sensor. Stanulis et al. [22] studied the structural and microstructural characteristics of the same compound obtained by gel to crystalline conversion method. Recently, our research group [23] reported the synthesis and the thermal behaviour of the SrSn$_{1-x}$Ti$_x$O$_3$ powders obtained by the polymeric precursor method. In relation to Sr(Sn,Ti)O$_3$ thin films, some related compositions have already been studied, such as (Sr$_{0.98}$Eu$_{0.02}$)$_2$(Sn$_{0.90}$Ti$_{0.10}$)O$_4$ [24] and

* Corresponding author at: Institut des Sciences Chimiques de Rennes, UMR 6226 CNRS/Université de Rennes 1, Campus de Beaulieu, 35042 Rennes Cedex, France.
E-mail address: andrel_ltm@hotmail.com (A.L. Menezes de Oliveira).

$(Ba_{0.70}Sr_{0.30})(Sn_{0.20}Ti_{0.80-x}Mn_x)O_3$ [25] obtained by pulsed laser deposition and $Ba_{0.50}Sr_{0.50}(Ti_{0.80}Sn_{0.20})O_3$, obtained by chemical solution deposition [26]. Only a very recent paper has reported the $SrSn_{1-x}Ti_xO_3$ solid solution in thin film form [27]. The authors have studied, in particular, the optical properties of films deposited on MgO by pulsed laser deposition.

In view of the literature data cited above, few compositions of the $SrTiO_3$–$SrSnO_3$ solid solutions were evaluated, most of them with substitutions also in the A site of the $ASn_{1-x}Ti_xO_3$ perovskite. However, technological applications of the $SrTiO_3$ and $SrSnO_3$ indicate that a more careful study about the solid solution would be of great worth. Indeed, the combination of $SrTiO_3$ and $SrSnO_3$ might allow tuning properties. For this purpose, structural and microstructure evaluations of this solid solution in thin film form is necessary in order to understand its properties. Although the preparation of $SrSn_{1-x}Ti_xO_3$ films by pulsed laser deposition (PLD) on MgO substrates has been previously reported in the literature [27], the influence of other parameters such as deposition method and nature of the substrates have not been explored yet and comparison among other data published in literature is not possible due to differences in composition, deposition methods and substrates. In fact, it is well established that the nature of the substrate determines the type of growth (polycrystalline or epitaxial) and consequently affected the microstructure and properties of the film. This means that by choosing appropriate substrates, epitaxial and polycrystalline thin films with diversified microstructures and properties can be obtained. The method used for deposition can also strongly influences the characteristics of the films [28,29]. It is therefore of great interest to explore different deposition methods in order to evaluate their effect on the structural and morphological properties of $SrSn_{1-x}Ti_xO_3$ thin films. The PLD is an attractive physical deposition method, which allows preparing highly epitaxial thin films (when appropriate substrate is used) with an accurate composition and growth control, besides favoring good adhesion of the film on substrate. On the other hand, chemical solution deposition (CSD) is attractive for the synthesis of thin films, especially for economic reasons, as it is a low cost process and allows the deposition on large area and complex shape substrates. Besides of these advantages, the CSD method allows the preparation of films with accurate stoichiometric control at low temperatures and the equipment used for deposition is much more simple, which does not require vacuum or atmosphere control. In relation to crystallization process, CSD is a soft process associated with a low energetic balance, in contrast with pulsed laser deposition that is energetic as well for the evaporation step of the material as for the crystallization that occurs in-situ at high temperature.

In this sense, the present work aims to perform a systematic investigation on the structural (in particular orientation) and microstructural evolution (in particular grain shape, growth and density), besides the photoluminescent properties (PL) in $SrSn_{1-x}Ti_xO_3$ thin films under the influence of the substrate, deposition method and composition. Photoluminescence characterization is an important tool for evaluating the presence of defects in wide band gap semiconductor materials, such as $SrTiO_3$ and $SrSnO_3$. To the best of our knowledge, these parameters were not yet evaluated for $SrSn_{1-x}Ti_xO_3$ solid solution based thin films.

2. Experimental details

Thin films of $SrSn_{1-x}Ti_xO_3$ (SST), with x = 0, 0.25, 0.50, 0.75 and 1 (named as SSO, SST25, SST50, SST75 and STO, respectively) were deposited on two single crystal substrates, alpha-Al_2O_3 and $LaAlO_3$, both with $(01\bar{1}2)$ orientation. Alpha-Al_2O_3 $(01\bar{1}2)$ is commonly called R-plane sapphire, while $(01\bar{1}2)$-oriented $LaAlO_3$ (LAO) is usually called (100) LAO due to its pseudocubic symmetry transformation,

for crystallographic simplification reason. In spite of presenting the same orientation, mismatch values between each of these substrates and the films are rather different and may lead to different behaviours in relation to the film orientation. For instance, (100) LAO is one of the most used substrates for presenting a quite small lattice mismatch with $SrTiO_3$.

Two different deposition methods were used: chemical solution deposition (CSD), a "soft" chemical process, and pulsed laser deposition (PLD), a physical process. It is worthy to note that the annealing temperature of the CSD method and the substrate temperature for PLD were previously optimized for SSO by our research group [28,29].

2.1. SST thin films synthesis by chemical solution deposition

SST coating solutions were prepared by the polymeric precursor method, which is a slightly modified Pechini process [30]. This method consists in chelating metallic cations with citric acid in an aqueous solution. Then these metal citrates polymerize with ethylene glycol by increasing the temperature. The precursors used in this present study were strontium nitrate (Sr(NO$_3$)$_2$ *Alfa Aesar*), tin chloride (SnCl$_2$·2H$_2$O *J.T. Backer*), titanium isopropoxide (Ti[OCH(CH$_3$)$_2$]$_4$ *Hulls-AG*), monohydrated citric acid (C$_6$H$_8$O$_7$·H$_2$O *Acros*) and ethylene glycol (C$_2$H$_6$O$_2$ *Acros*). The precursor solutions of each metal were prepared by adding the metal salts into a citric acid aqueous solution with 3:1 (citric acid:metal) molar ratio and ethylene glycol with 40:60 mass ratio (ethylene glycol:citric acid) under heating (353 K) and constant stirring, according to the procedure described in our previous work [23].

The temperature was raised up to about 363 K to obtain the different polymeric resins in agreement with the desired compositions. The viscosities of the resulting resins were then adjusted in the range of 25–30 mPa·s controlling the water content using a Brookfield DVII + Pro viscometer. From these solutions the films were spin coated at 105 rad·s^{-1} for 3 s and 314 rad·s^{-1} for 20 s (Spin Coater model KW-4A Chemat Technology). Only one layer was deposited for each film. The wet films were then submitted to two successive thermal treatments. In the first step, the samples were heat treated at 673 K for 2 h to eliminate the organic material, and then crystallized at 923 K for 2 h in air. These synthesis conditions led to the formation of thin films with a thickness (measured by FE-SEM) ranging from 250 to 280 nm (260, 250, 250 nm respectively for SSO, SST50 and STO films on sapphire and 250, 270, 280 nm respectively for SSO, SST50 and STO films on LAO).

2.2. SST thin films synthesis by pulsed laser deposition

For PLD synthesis, homemade sintered targets were prepared by solid-state reaction using stoichiometric amounts of strontium carbonate (SrCO$_3$ *Merck*), tin oxide (SnO$_2$ *Aldrich*) and titanium oxide (TiO$_2$ *Alfa Aesar*) as starting materials to obtain the desired compositions. Characterizations by X-ray diffraction and Energy Dispersive Spectroscopy analyses performed on the different targets have confirmed that the expected single-phase perovskite is obtained with the desired composition (Fig. S1 to S2 and Table S1 of the Supplementary information).

SST thin films were grown at 973 K for 30 min under an oxygen pressure of 30 Pa, using a KrF excimer laser (λ = 248 nm, f = 2 Hz, 210 mJ/pulse) with a substrate-target distance fixed at 55 mm. These deposition conditions allowed obtaining thin films with a thickness (measured by FE-SEM) varying from 210 to 280 nm (280, 240, 210 nm respectively for SSO, SST50 and STO films on sapphire and 275, 260, 270 nm respectively for SSO, SST50 and STO films on LAO).

2.3. Thin film characterizations

The structural characteristics were analyzed using X-Ray diffraction (XRD). Standard θ–2θ scans were performed with a two-circle Bruker D8 Advance diffractometer using the monochromatized Cu K$_{\alpha1}$

Table 1
Structural informations for SSO, STO, sapphire and LAO.

Compounds	Space group	Lattice parameter (Å)	Pseudo-cubic lattice parameters (Å)	Transformation matrix
SrSnO₃	Pbnm [6]	$a = 5.707(2)$ $b = 5.707(2)$ $c = 8.064(2)$	$a_{pc} = b_{pc} = 4.035$ $c_{pc} = 4.032$ $\gamma_{pc} = 90.00°$ $\langle a_{pc} \rangle = 4.034$	$\begin{pmatrix} 1 & 1 & 0 \\ -1 & 1 & 0 \\ 0 & 0 & 2 \end{pmatrix}_{p \to o}$
SrTiO₃	Pm$\bar{3}$m [1]	$a = 3.9050$ (± 0.0004)	$a = 3.905$	
Alpha-Al₂O₃ (sapphire)	R$\bar{3}$c [33]	$a = 4.760$ $c = 12.993$	$a_{pc} = 3.500$ $\alpha_{pc} = 85.75°$	$\begin{pmatrix} -1 & 1 & 0 \\ 0 & -1 & 1 \\ 2 & 2 & 2 \end{pmatrix}_{p \to h}$
LAO	R$\bar{3}$c [34]	$a = 5.3655(2)$ $c = 13.112(1)$	$a_{pc} = 3.791$ $\alpha_{pc} = 90.10$	$\begin{pmatrix} -1 & 1 & 0 \\ 0 & -1 & 1 \\ 2 & 2 & 2 \end{pmatrix}_{p \to h}$

Legend: $\langle \rangle$ average value, "o" orthorhombic, "h" hexagonal and "p" pseudocubic.
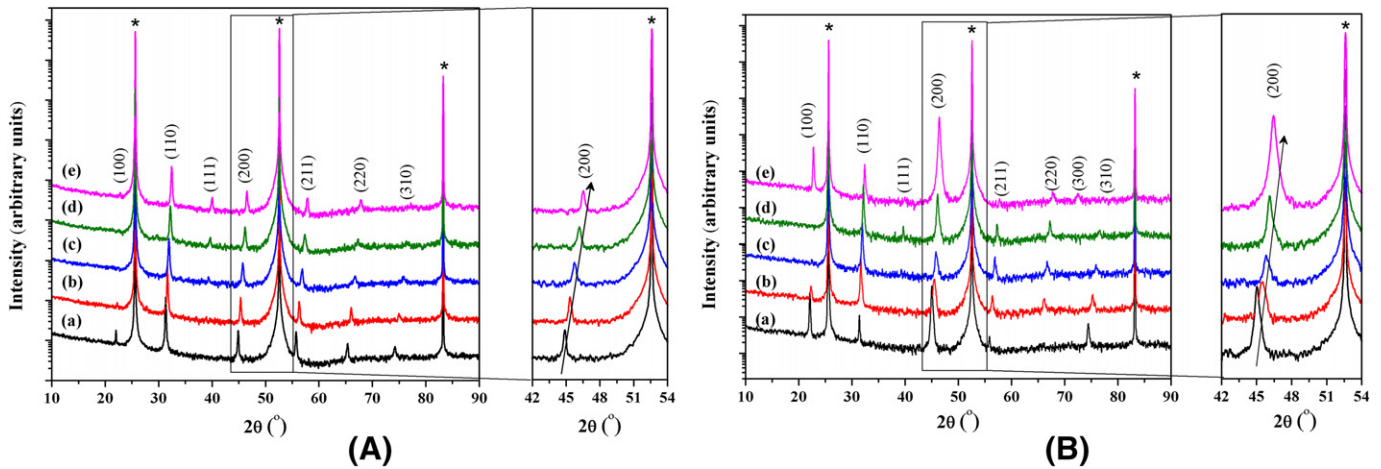

Fig. 1. θ–2θ XRD patterns (in log scale) of the SSO (a), SST25 (b), SST50 (c), SST75 (d), and STO (e) thin films deposited on R-sapphire by: (A) CSD and (B) PLD. Peaks marked with (*) are assigned to the substrate.

radiation. The ω-scans (used to evaluate the crystalline quality along the growth direction) and φ-scans (used to study the in-plane ordering) were recorded with a four-circle Bruker D8 Discover diffractometer operating with Cu K$_\alpha$ radiation. Thin film microstructures were observed with a field emission scanning electron microscope (FE-SEM, Jeol 6301-F) which was operated at low voltage, typically 7–9 kV to limit charge effects and to achieve high resolution without requiring surface metallization. Measurement of the thickness was done by evaluation of the film cross section by FE-SEM. Surface roughness of the films was acquired using an atomic force miscroscope (AFM, Cypher Atomic Force Microscope, Asylum Research Oxford Instruments) in AC mode with silicon point probe (AC160TS-R3, Olympus). Photoluminescence (PL) measurements were carried out at room temperature using a spectrophotometer (Thermal Jarrel-Ash Monospec 27, USA) with the monochromator coupled to a photomultiplier (Hamamatsu R446, Japan). A 350.7 nm krypton ion laser (Coherent Innova 90 K, USA) was used as the excitation source using a maximum output power of 250 mW.

3. Results and discussion

It is known that the crystalline structures of SrSnO₃ (SSO, ICDD 22-1798) and SrTiO₃ (STO, ICDD 35-0734) are orthorhombic and cubic, respectively. In order to compare the cell parameters in the SST solid solution, a pseudo-cubic cell was considered for SrSnO₃. The pseudocubic cell can be obtained by a transformation matrix on the basis of the reciprocal lattice vectors of the original perovskite unit cell as shown in Table 1. For SrSnO₃, which adopts an orthorhombic structure at room temperature, a reduced cell can be considered by converting the original orthorhombic lattice parameters (a_o, b_o and c_o) to the length of the equivalent primitive unit cell, i.e. pseudocubic (a_{pc}). The reduced lattice parameters (a_{pc}) are then obtained using the correlation $a_{pc} \approx \frac{a_o}{\sqrt{2}} \approx \frac{b_o}{\sqrt{2}} \approx \frac{c_o}{2}$ [31,32].

Table 1 shows the structural parameters for both oxides, SSO and STO, as well as for both substrates (LAO and sapphire). In this present work, we used the Miller-Bravais indices of the hexagonal

Table 2
Lattice parameters a_{pc} (Å) observed for the SST thin films grown on R-sapphire and on LAO by CSD and PLD.

Thin films	on R-sapphire				LAO			
	CSD	FT (nm)	PLD	FT (nm)	CSD	FT (nm)	PLD	FT (nm)
SSO	4.041 ± 0.001	260	4.029 ± 0.003	280	4.029 ± 0.001	250	4.024 ± 0.004	275
SST25	4.002 ± 0.001	–	3.992 ± 0.005	–	3.988 ± 0.001	–	3.992 ± 0.003	–
SST50	3.967 ± 0.001	250	3.962 ± 0.004	240	3.964 ± 0.002	270	3.961 ± 0.001	260
SST75	3.936 ± 0.002	–	3.936 ± 0.001	–	3.932 ± 0.001	–	3.935 ± 0.003	–
STO	3.906 ± 0.001	250	3.911 ± 0.002	210	3.904 ± 0.001	280	3.917 ± 0.004	270

Legend: "FT" film thickness.

Table 3
Mismatch values calculated for SSO and STO thin films on R-sapphire substrate. (R-plane sapphire parameters: 4.76 Å // [100] and 15.389 Å // [12$\bar{1}$]; The mismatch values in the [12$\bar{1}$] direction were calculated with 15.389 / 3 = 5,13 Å).

Compound	Lattice parameter a_p (Å)	Mismatch with sapphire (%) [12$\bar{1}$]/[100] directions
SSO	4.035	−21.3/−15.2
STO	3.905	−23.9/−17.9

Compound	Lattice parameter $a_p\sqrt{2}$ (Å)	Mismatch with sapphire (%) [12$\bar{1}$]/[100] directions
SSO	5.706	11.2/19.9
STO	5.522	7.6/16.0

setting for R-sapphire and Miller indices of the pseudo-cubic cell for LAO.

3.1. SST thin films grown on R-sapphire substrates

The θ–2θ XRD patterns of the SST films grown by CSD and PLD on R-sapphire are shown in the Fig. 1A and B. In both cases, all of the compositions have a perovskite single-phase structure. For comparison, all of the diffraction peaks were indexed considering a pseudo-cubic unit-cell, with lattice parameters presented in Table 2. As expected, a shift of the Bragg angles to the higher 2θ values is observed as Ti content increases, indicating that a decrease of the a_{pc} lattice parameter occurs. This decrease can be attributed to a decrease of the cation average size (r_{Ti} = 0.605 Å; r_{Sn} = 0.690 Å) [35] which promotes a contraction of the lattice as predicted by the Vegard Law [36,37]. Moreover, a higher covalent character is expected for Ti^{4+}-O^{2-} bond comparing to Sn^{4+}-O^{2-}. The decrease of the lattice parameter according to the Ti content was observed by Zhai et al. [18] for Ba(Sn$_x$Ti$_{1-x}$)O$_3$ thin films grown by the sol-gel route. It was also reported on bulk for other Ti-based oxide systems [14,38] and for the same Sr(Sn,Ti)O$_3$ ceramic system [21,22]. Liu et al. [27] also observed the same behaviour for SrSn$_{1-x}$Ti$_x$O$_3$ thin films deposited by PLD on MgO.

The θ–2θ XRD patterns (Fig. 1A and B) also revealed a randomly oriented growth for CSD films (polycrystalline growth) whereas the PLD ones tend to present a (h00) oriented growth (peaks of this family are

more intense), especially for the STO composition. As no major difference is observed in thickness for the majority of SST films obtained by PLD and CSD (for example 20 nm of difference for SSO and 10 nm of difference for STT50), the preferential orientation for PLD films may be assigned to the highest deposition temperature used for this process (973 K) compared to the annealing temperature used for the CSD method (923 K) but also to the nucleation grain growth process which is different from the CSD one, as explained later.

The φ-scans performed of the 110 reflections of the SSO, SST25, SST50 and SST75 grown by PLD (no φ-scans were performed on these compositions prepared by CSD because of the randomly growth orientation observed in the θ–2θ XRD patterns) indicate that no in-plane ordering occurs (flat phi-scans, not shown here). The same result was also observed by Alves et al. [28] for SrSnO$_3$ thin film deposited on R-sapphire. This behaviour can be explained by several reasons – the large mismatch between films and substrate (Table 3), the distortion of the oxygen network of R-sapphire [39,40] and the highest difficulty to grow high quality thin films from solid-solution than from defined compounds, due to cationic disorder.

As previously mentioned, among the films deposited by PLD, the STO one presents the higher (h00) preferential orientation. The ω-scan performed for this film (Fig. 2A) shows an out-of-plane ordering with a value of full width at half maximum Δω = 3.11°. This relatively high value reflecting mosaicity is not surprising considering the mismatch values between STO and the R-plane sapphire (Table 3) and also the presence of other orientations than (100). The phi-scan performed of the 110 reflections of this STO film grown by PLD shows 4 peaks equally separated from each other by 90° in agreement to the STO cubic structure evidencing the in-plane ordering of this film (Fig. 2B). It can be observed in Fig. 2B that the STO reflections are shifted by 45° with respect to the 006 reflection of the R-sapphire substrate, meaning that the [011] direction of the STO film is parallel to the [12$\bar{1}$] direction of the substrate. This in-plane ordering observed for the STO film grown by PLD, whose modelling is shown in Fig. 3, is explained by the smaller value of the mismatch obtained with this alignment (comparison of the mismatches calculated with the lattice parameter a_p and the lattice parameter $a_p\sqrt{2}$ of STO, Table 3). However, a quite large value of Δφ (4.6°) is observed which appears related to the angular differences between the (01$\bar{1}$2) Al sublattice of sapphire and the (100) Ti sublattice of the STO thin film. Fig. 4 shows three possible local in-plane arrangements of the Ti sublattice on the Al one. The first arrangement (Fig. 4a)
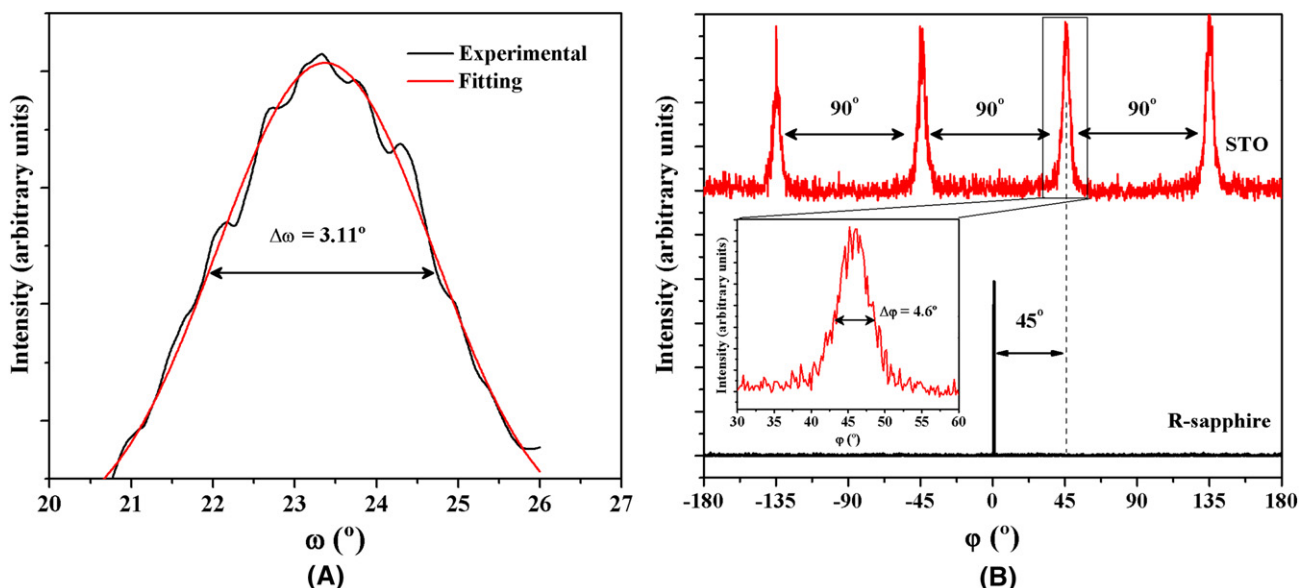

Fig. 2. XRD patterns of the STO thin film deposited on R-sapphire by PLD: ω-scan of the 200 STO peak (A) and φ-scan of 110 STO and 006 sapphire reflections (B).
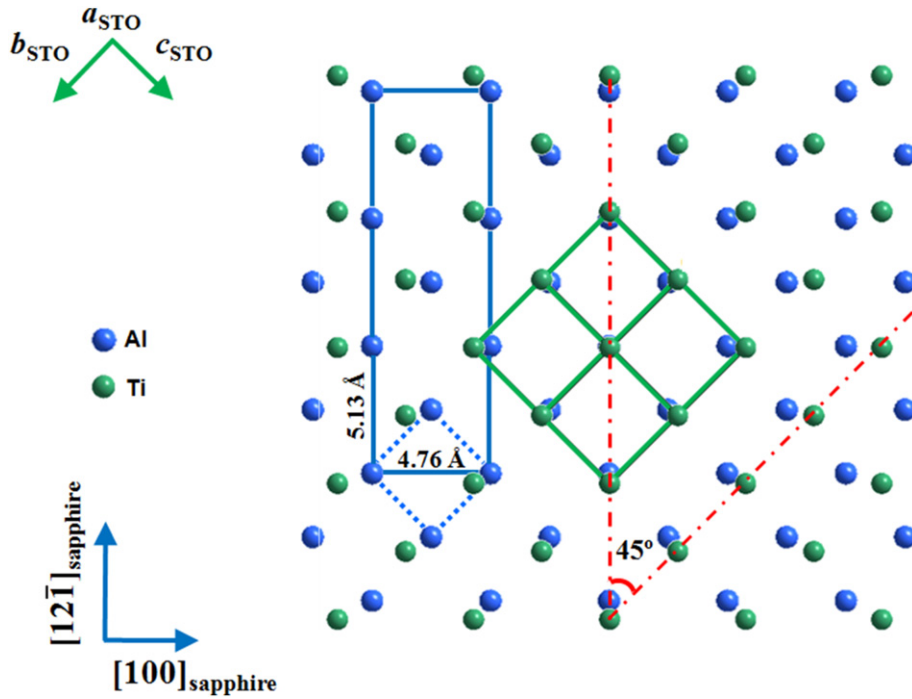
Fig. 3. Schematic of proposed disposition between STO thin film and R-sapphire substrate (the figure shows only Ti and Al sublattices for more clarity). Solid blue line represents the unit cell of sapphire R-plane; dashed blue line represents the trace on the latter of the pseudo-cubic unit cell of sapphire; green line represents the trace of the STO unit cell.

represents the "b_{STO}" direction aligned on the [$\overline{2}2\overline{1}$] sapphire direction, the second one (Fig. 4b) shows the theoretically expected epitaxy (alignment of [011] STO on [$12\overline{1}$] sapphire direction) and the last one (Fig. 4c) represents the "c_{STO}" aligned on the [$42\overline{1}$] sapphire direction. These three possible alignments result in the theoretical angular amplitude of 4.30° which is close to the experimental value of $\Delta\varphi = 4.6°$ observed on φ-scan, meaning that these three arrangements

may exist simultaneously in different regions of the (100) STO plane on the (01$\overline{1}$2) sapphire one.

The absence of in-plane ordering for STO deposited by CSD may be explained by the nucleation/grain growth process that is different from the PLD method. PLD is an in-situ deposition method, i.e. crystallization occurs directly from the vapor phase on the heated substrate. The film grows directly atom by atom from the interface, the impinging
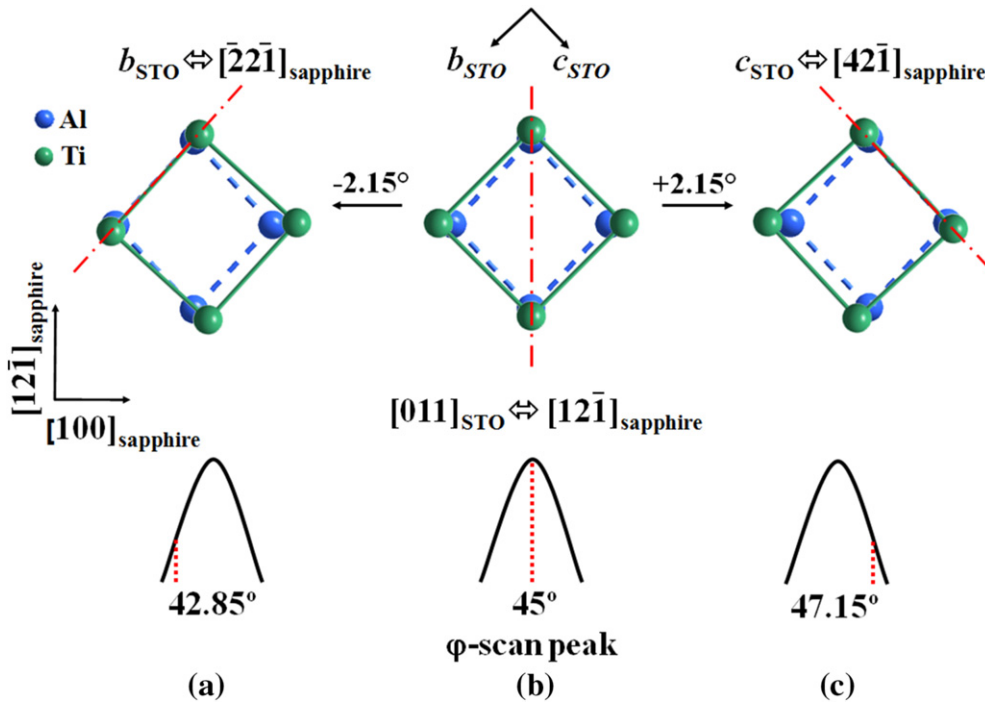

Fig. 4. Schematic views of the STO (100) plane disposed on the sapphire (01 − 12) one. α_{STO} − angle$_{Sapphire}$ = 4.30° (theoretical value) ⟺ $\Delta\varphi$ = 4.6° (experimental value).
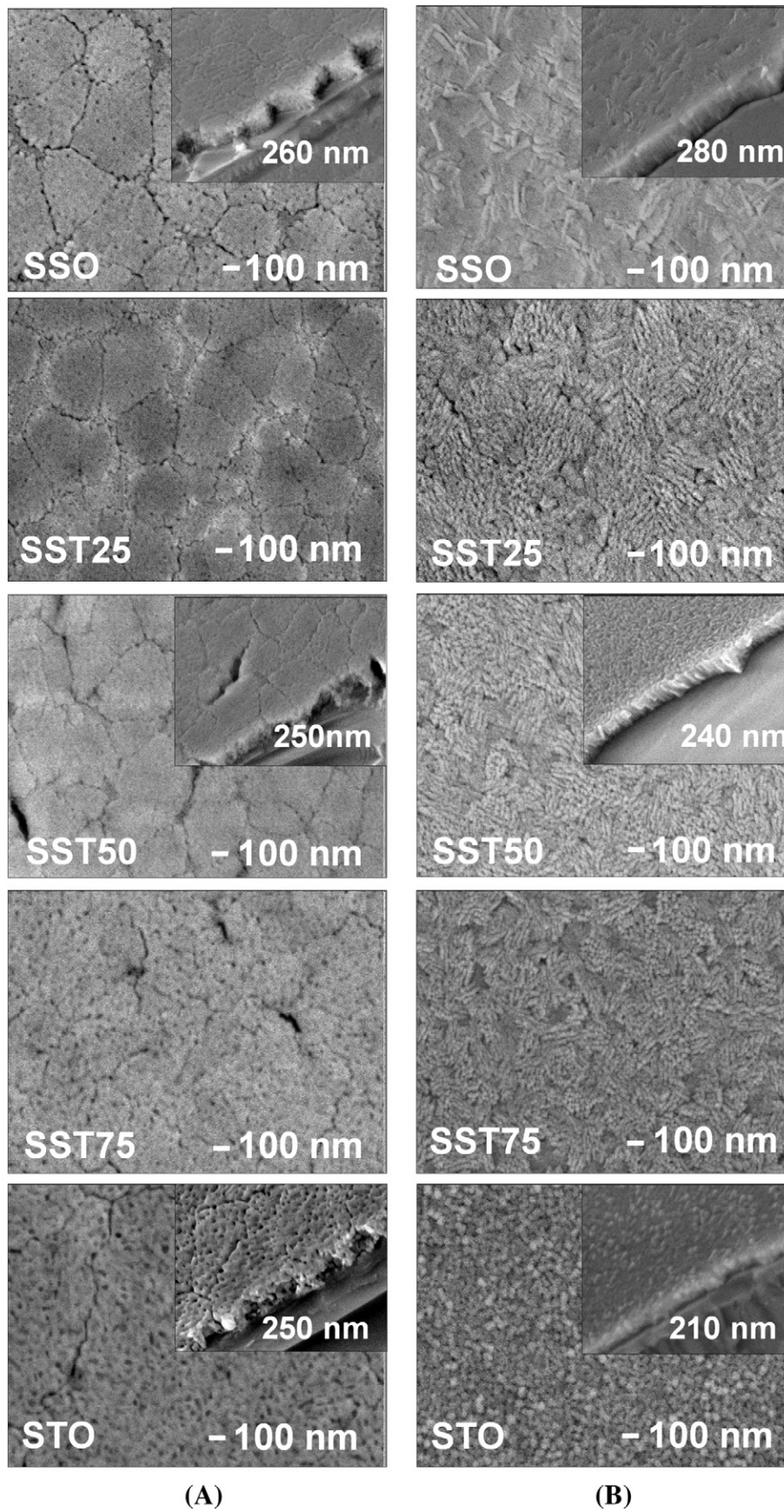
Fig. 5. FE-SEM images of SST thin films deposited on R-sapphire by CSD (A) and PLD (B). The film thicknesses are given in the insets for the micrographs of the SSO, SST50 and STO thin films.

atoms having sufficient thermal energy to move on the surface and to reach an energy well. Then, in favorable conditions (low misfit, similar structure) the film orients itself to minimize interfacial energy. For CSD films, the nucleation/grain growth process (usually associated to long-range ordering) occurs after deposition, during the post-annealing treatment of the film obtained from a solution which already has some short-range order [41]. There are at first a lot of randomly oriented nuclei in the bulk of the crystallizing film. Then, but only in very favorable conditions, the growing grains (at or near the interface) that are aligned with the substrate are energetically favored. In a further step, all the grains can take this orientation by a mechanism of Ostwald ripening. This different nucleation/grain growth process explains the difficulty to obtain in-plane ordering for a CSD film in the case of a relatively

high film-substrate mismatch (case of STO on R-sapphire), unlike the PLD one.

The FE-SEM images of the SST films deposited on R-sapphire using CSD and PLD are displayed in Fig. 5A and B, respectively. It can be observed that the microstructure of the films is strongly influenced by the composition and method of deposition. As no major difference is observed in thickness for the majority of SST films obtained by PLD and CSD, this difference in the morphology is mainly due to other factors.

The films deposited by CSD (Fig. 5A) are more porous than the PLD ones (Fig. 5B), for all of the compositions, probably due to the elimination of H_2O and CO_2 during decomposition of the polymeric network. The presence of pores in the thin films deposited by CSD may be interesting for applications as catalysis, photocatalysis and adsorbent
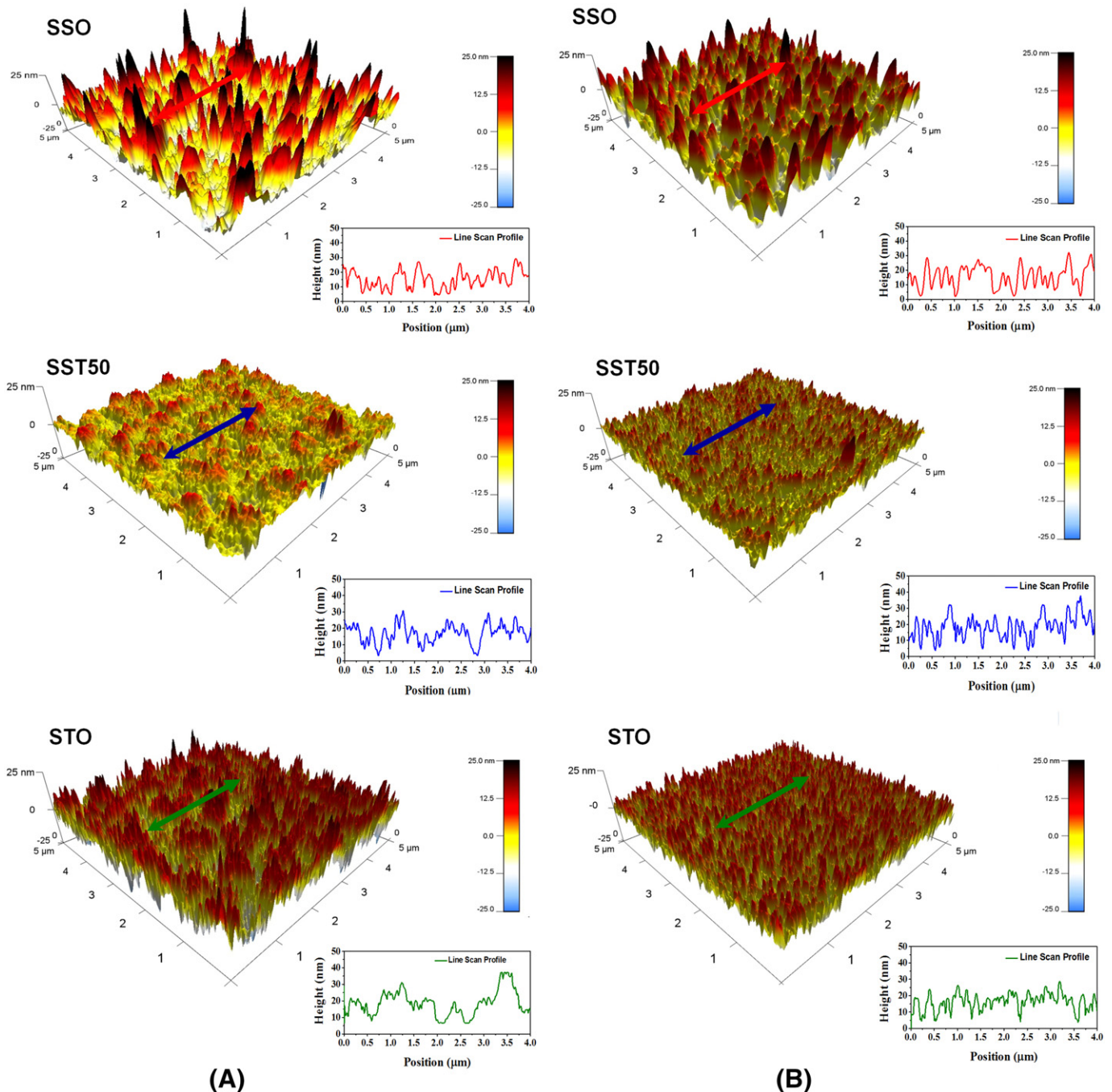

Fig. 6. AFM images of SST thin films deposited on R-sapphire by CSD (A) and PLD (B).
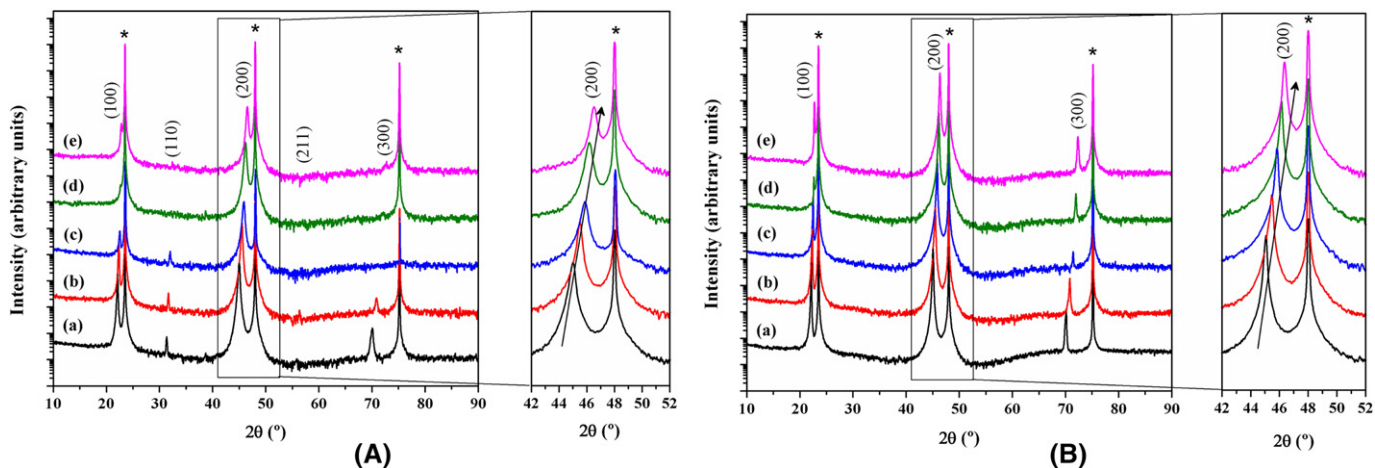
Fig. 7. θ–2θ XRD patterns (in log scale) of the SSO (a), SST25 (b), SST50 (c), SST75 (d), and STO (e) thin films deposited on (100) LAO by CSD (A) and PLD (B). Peaks marked with (*) are related to the substrate.

materials. For these films obtained by CSD, a granular morphology is observed (as showed the FE-SEM cross sections of SSO, SST50 and STO in insets Fig. 5A), which differ according to the composition. As the film thickness is in the same range (260, 250 and 250 nm for SSO, SST50 and STO grown by CSD respectively), the difference in the morphology in the CSD films may be thus mainly assigned to the difference in the crystallization and nucleation/grain growth processes according to the composition, as discussed by Alves et al. for $SrSnO_3$ and $CaSnO_3$ thin films synthesized by the same method [29]. The grains size was evaluated to around 26 nm for the STO film grown by CSD (for the other compositions, it was difficult to evaluate the grain size because these ones are not well defined).

The films obtained by PLD (Fig. 5B) exhibit microstructures strongly different from those deposited by CSD (Fig. 5A). As previously mentioned, no major difference is observed in thickness for the majority of SST films obtained by PLD and CSD (for example 20 nm of difference for SSO and 10 nm of difference for STT50), the change of morphology for a same composition may be thus mainly attributed to the difference in the nucleation/grain growth processes of the two methods as described before (in the discussion on the XRD patterns). The influence of the type of growth (randomly oriented growth for CSD films and (h00) preferential oriented growth for PLD films) on the microstructure cannot be totally excluded. The columnar growth observed on the FE-SEM cross sections of SSO, SST50 and STO deposited by PLD (insets of Fig. 5B) confirms this difference of nucleation/grain growth processes (granular growth in case of

CSD films). The surface morphology of the PLD films revealed irregular and elongated grains for all of the compositions except for STO which presents small round grains which size is evaluated to around 22 nm (comparable with the size of STO film obtained by CSD).

The change of microstructure of thin films deposited by PLD according to the composition can be explained in terms of kinetic properties of the species appearing on the surface substrate during the deposition. The ablated species, after being ejected from the target, lose kinetic energy, which is essentially due to scattering by the oxygen molecules inside the chamber. Under oxygen atmosphere, the different species reach the substrate with different kinetic energy; therefore, their surface mobility decreases if the species present a lower kinetic energy, which involves a smaller grain size. As result, a high amount of nucleation sites normally spherical are created with the dimension of few nanometers. On the other hand, species which have not yet thermally accommodated on the substrate, execute random diffusive jumps and then interact to others, which lead to the formation of bigger nucleation sites forming big particles with irregular shape [42,43].

These results show that the nucleation/ grain growth processes, which depend on the composition, but also on the deposition method, strongly influences the film morphology. The AFM images obtained with a scanning area of 5 × 5 μm^2 of the SST thin films grown by both methods confirms these results (Fig. 6A and B). In addition, the root mean square surface roughness values (R_{RMS}) and the average roughness (R_a) of the films decreases with the increase of Ti content whatever the method
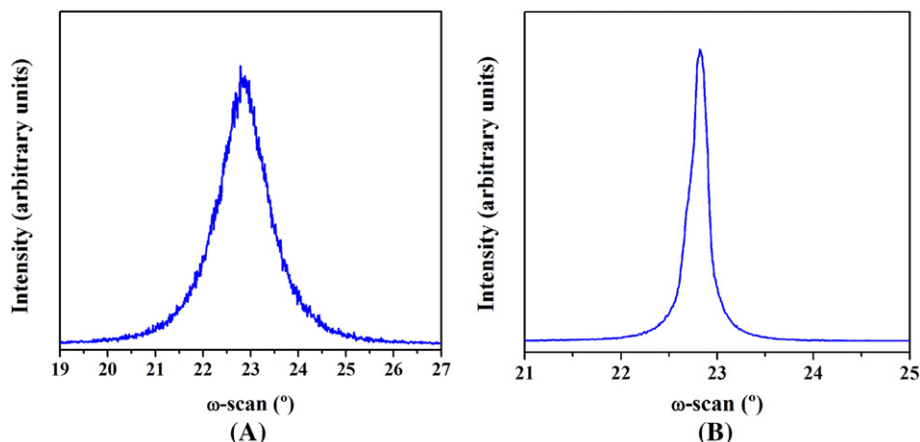

Fig. 8. ω-scans of the 200 reflection of the SST50 thin films deposited on (100) LAO by CSD (A) and PLD (B).

Table 4
Out-of-plane ($\Delta\omega$) and in-plane ($\Delta\varphi$) values for the SST thin films obtained by CSD and PLD on LAO substrate. The thickness of the films is given for the SSO, SST50 and STO compositions.

Thin films	CSD				PLD		
	$\Delta\omega$-scan		$\Delta\varphi$-scan		$\Delta\omega$-scan		$\Delta\varphi$-scan
	Film	Substrate	Film		Film	Substrate	Film
SSO	0.83°	0.02°	1.6°		0.20°	0.04°[b]	1.3°
SST25	0.13°	0.06°	1.4°		0.09°	0.08°	1.4°
SST50	1.07°	0.15°[a]	1.9°		0.23°	0.14°[a]	1.2°
SST75	1.60°	0.05°[b]	2.8°		0.29°	0.20°[a]	1.2°
STO	3.07°	0.04°[b]	1.9°		0.22°	0.10°	1.4°

[a] Asymmetrical peak.
[b] Rocking curve presenting peaks of very small intensity (with $\Delta\omega \sim 0.03°$) around the main peak.

used for deposition: R_{RMS} = 8.8, 6.5, 3.6 nm for the SSO, SST50 and STO films grown by CSD and 6.6, 4.3 and 3.5 nm for those deposited by PLD, respectively. Through the profile of the linescan curves extracted from the AFM images, the SSO, SST50 and STO films deposited by CSD showed a R_a roughness of 7.0, 5.2 and 2.9 nm, respectively, while the R_a values of those films deposited by PLD were measured to be 5.2, 3.5 and 2.7 nm, respectively. The decrease in the roughness values for $SrSn_{1-x}Ti_xO_3$ thin films was also observed by Liu et al. with films deposited by PLD on (001) MgO [27]. Moreover, it can be observed that both R_{RMS} and R_a values tend to be lower for PLD films which suggests that smoother films may be obtained by this method compared to CSD ones.

3.2. SST thin films grown on (100) LAO substrates

The θ–2θ XRD patterns of the SST thin films grown on (100) LAO are shown in the Fig. 7A and B. All of the films are single-phase with a high (h00) orientation. When the SST thin films are prepared by CSD, a very small 110 peak is observed for the SSO, SST25 and SST50 compositions, but is not detected in SST75 and STO. Sharper and more intense peaks are observed for the PLD samples suggesting a higher crystallinity for these films compared to CSD ones. No meaningful difference is observed comparing thicknesses of the films obtained by PLD or CSD. For STO and SST50, only 10 nm of difference was observed, while 25 nm of difference

was measured for SSO. The higher crystallinity of the films obtained by PLD may be assigned to the highest deposition temperature of the PLD method (973 K), compared to the annealing temperature used during the CSD method (923 K). Moreover, during PLD the deposition occurs in situ, i.e., the species of the target (atoms and ions) are ejected under oxygen atmosphere with a high kinetic energy. These species migrate to substrate with a higher surface mobility where they condense and solidify, building up one atomic layer at a time [42,43]. This induces a higher ordering arrangement of the atoms of the material that is being deposited. As consequence the diffraction peaks in the diffraction pattern tend to be intense and sharp, indicating a high long range order of the film.

As previously observed for the films grown on R-sapphire, a shift of the Bragg angles to the higher 2θ values is observed as Ti content increases, leading to a decrease of the a_{pc} lattice parameter (Table 2).

The ω-scans performed around the 002 SST peak confirm a high out-of-plane orientation for all of the samples. As examples, the ω-scans obtained for the SST50 films are shown in Fig. 8A and B. The FWHM values ($\Delta\omega$) tend to increase with the Ti content for the CSD films (Table 4). This result is quite surprising considering the mismatch values between the films and the substrate: 6.5% for SSO and 3.1% for STO. However, the $\Delta\omega$ value may sometimes be higher due to the twinned structure of LAO substrates [44]. Indeed, some ω-scans performed around the 200 peak of LAO (not shown here) presented an asymmetrical shape or peaks of very small intensity around the main peak, leading to larger $\Delta\omega$ values for the corresponding films. Comparing the two methods of deposition, a higher out-of-plane orientation is observed for all of the films synthesized by PLD, confirming higher crystalline quality and orientation, in agreement with the θ–2θ patterns observations.

It has already been reported in the literature that STO [45,46] and SSO [28] thin films can grow epitaxially on (100) LAO by PLD. As expected in the present work, the films based on the SST solid solution also present an epitaxial growth on (100) LAO substrate, as shown by the presence of 4 peaks in the φ-scans separated from each other by 90° (Fig. 9A and B). These diffraction peaks arise at the same azimuth as the 110 peaks of the substrate, indicating that SST thin films were epitaxially grown on top of the (100) LAO substrate plane, with a like cube-on-cube epitaxy. The in-plane relationship between the SST thin film and the LAO substrate is therefore $\langle010\rangle_{SST}$ // $\langle010\rangle_{LAO}$. In contrast to the growth on R-sapphire, epitaxy on (100) LAO is favored by a
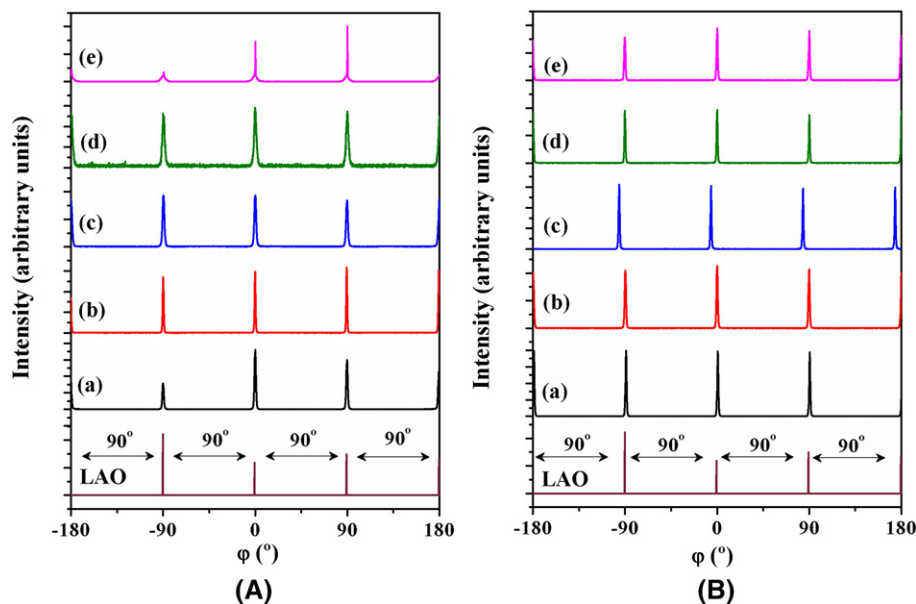

Fig. 9. φ-scans of the 110 reflection of the LAO substrate and of the 110 reflection of the SSO (a), SST25 (b), SST50 (c), SST75 (d), and STO (e) thin films deposited on (100) LAO by CSD (A) and PLD (B).
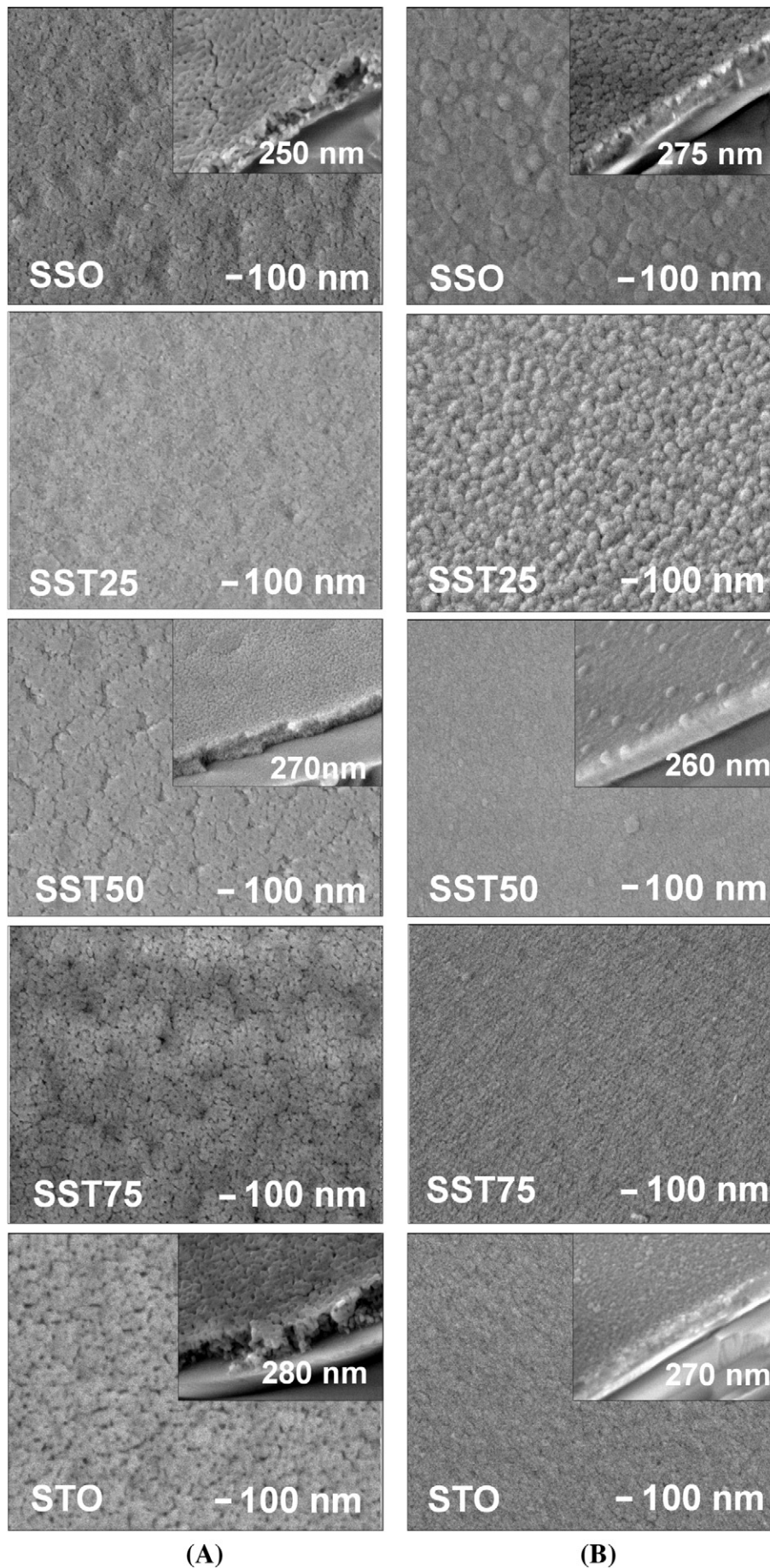
Fig. 10. FE-SEM images for SST thin films grown on (100) LAO by CSD (A) and PLD (B). The film thicknesses are given in the insets for the micrographs of the SSO, SST50 and STO thin films.
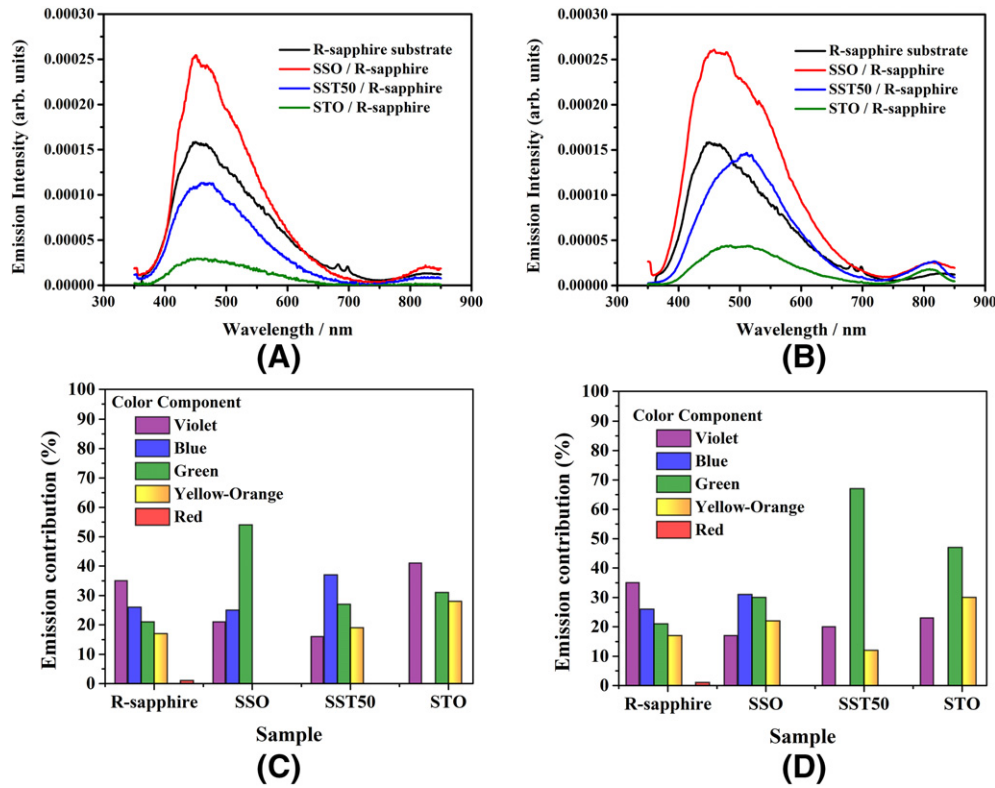
Fig. 11. Photoluminescence spectra and band emission contribution of the SSO, SST50 and STO films grown on R-sapphire deposited by CSD (A, C) and PLD (B, D).

lower mismatch value between SST thin films and LAO substrate (3.1% for STO on LAO and 6.5% for SSO on LAO). In addition, the mechanism of individual cluster rotation due to lattice network distortion does not occur anymore in case of (100) LAO (the angular mismatch between

the film and the LAO substrate is very small (≤0.1%) for all of the compositions). As a result, the φ–scan peaks are considerably narrower in this case, compared to the ones obtained on the STO film synthesized by PLD on R-sapphire. The Δφ values, which are representative of the
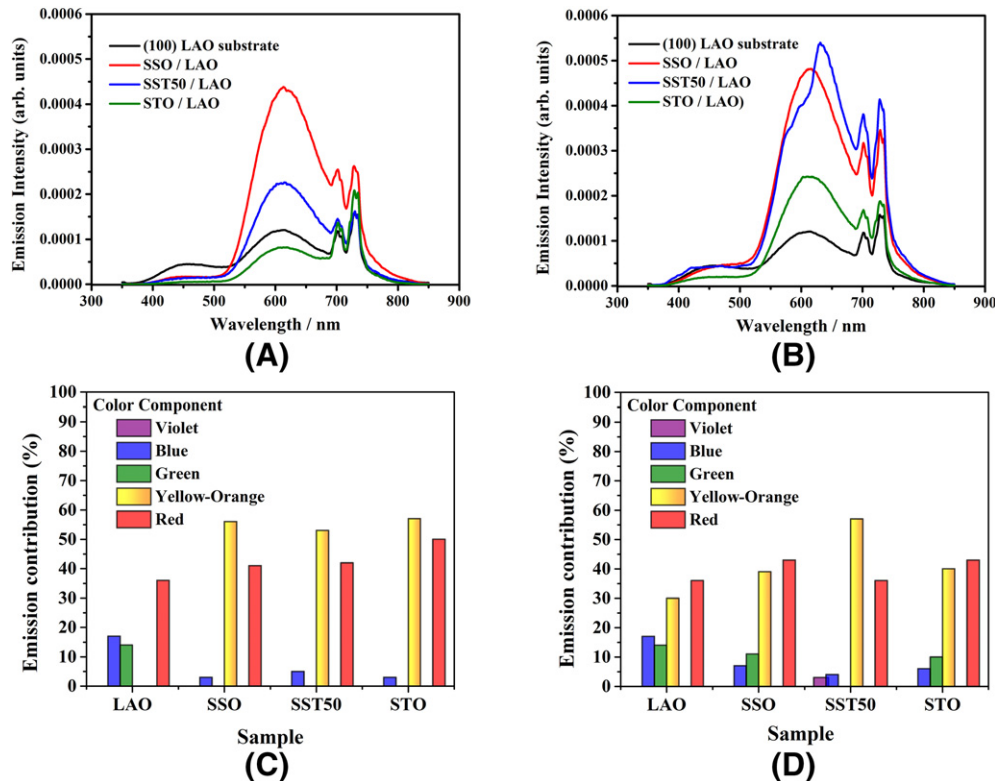

Fig. 12. Photoluminescence spectra and band emission contribution of the SSO, SST50 and STO films grown on LAO deposited by CSD (A, C) and PLD (B, D).

quality of the alignment at the interface and not sensitive to the parameter mismatch (provided that the latter allows epitaxial growth), are quite similar for all of the SST films deposited on LAO (Table 4), confirming the high quality of the epitaxial growth.

Fig. 10A and B show the morphology of the SST thin films grown by CSD and PLD, respectively. All of the films are homogeneous and crack-free, but the morphology is greatly influenced by the deposition method and by the increase of Ti content, as previously observed for the SST thin films on sapphire. The films deposited by CSD are more porous assigned to the decomposition of the polymeric network during the heat treatment, as previously discussed. The presence of Ti^{4+} in the SST films deposited by PLD induces the decrease of the grain size, more visible on LAO substrates because the grains are round for all of the compositions (showing that other factors than kinetic properties of the species during the PLD deposition influence the grain shape). This size decrease (grain size of 87 nm, 55 nm and 19 nm for SSO, STT50 and STO respectively for PLD films on LAO) may be correlated with the amount of nuclei created during the PLD process. The smaller grain sizes observed for Ti-richer samples may be associated to a higher amount of created nuclei, while bigger grains of the Sn-rich thin films may be favored by a lower amount of nuclei which can thus grow more easily.

It can be also noted that for the same composition and for the same method of deposition, the morphology depends on the substrate used for deposition (comparison between Figs. 5A, B and 10A, B). The difference in morphology is assigned to the epitaxial growth of the films deposited on LAO, as crystallization process is changed.

3.3. Photoluminescence of the films grown on R-sapphire and LAO substrates

The photoluminescent (PL) spectra of the SSO, SST50 and STO thin films deposited on R-sapphire (Fig. 11A, B) and (100) LAO (Fig. 12A, B) substrates by CSD and PLD methods present a typical behaviour of multiphoton or multilevel processes. In this case the relaxation occurs by several pathways, which involve the participation of numerous energy sublevel states within the band gap [47–49]. PL can be originated from different type of short-range defects - shallow (energy states close to the valence or to the conduction band originated from less distorted structures) and deep ones (energy states close to the middle of the band gap due to highly distorted structures). According to Longo et al. [48,49], deep defects lead to a less energetic green-yellow-red emission, while shallow defects lead to a more energetic violet-blue emission.

As observed on Figs. 11A, B and 12A, B, the broad PL emission responses are dependent on the composition, nature of substrates, besides the method of deposition, and these responses occur at different wavelength in the range of 350–800 nm. In order to understand the different PL behaviours of the films, the PL spectra were deconvoluted into symmetric Gaussian functions. According to these data, the broad emission band was divided into three to five color components, which vary according to the composition, growth and deposition method. The contribution of each deconvoluted curve and its variation are shown in Figs. 11C, D and 12C, D. The deconvolution data are listed in Table S2 to S5 in the Supplementary information file.

Films deposited on (100) LAO (Fig. 12A, B) present a PL at a lower energy range i.e. longer wavelength (compared to the emissions from films grown on sapphire), which may be related to the creation of deep defects within the band gap of materials. Moreover, the Sn content in the lattice induces an increase of PL. The short-range disorder responsible for the distortion of the SST lattice deposited on the (100) LAO network favors PL, especially for SSO film that suffers higher distortion, probably due to its higher misfit compared to STO composition. The short-range disorder in the SST films on LAO lattice is responsible for the creation of energy levels within the bandgap, which leads to intense PL responses occurring mostly at lower energy range. On the other hand, the SST films grown on R-sapphire present bigger PL at higher

energy range (short wavelength), indicating the formation of shallow defects in the bandgap, probably due to its polycrystalline nature.

4. Conclusions

A detailed study about the influence of the composition, the substrate and the deposition method on the structural and microstructural characteristics of the films has been carried out in this article. On R-sapphire, SST randomly oriented (polycrystalline) thin films have grown by CSD whereas (h00) preferential oriented films were obtained by PLD. The STO film grown by PLD on sapphire exhibited an in-plane ordering (epitaxial growth) with [011] STO direction parallel to $[\,12\bar{1}\,]$ direction of the sapphire, meaning a rotation of 45° between the STO lattice and the sapphire one. The SST thin films grown on LAO were all highly a-axis oriented with a like cube-on-cube epitaxy, meaning $\langle 010 \rangle_{SST}$ // $\langle 010 \rangle_{LAO}$. All of the structural differences were explained on the basis of misfit considerations and interface arrangements. Moreover, the morphology of the SST thin films was strongly correlated to the nature of the substrate (which induces the type of growth) but also to the nucleation/grain growth processes which are different according to the composition and also to the deposition method. The PL observed in SST thin films was dependent on the composition and type of growth, which induce the creation of different types of defects within the bandgap. The higher energy emission was associated with shallow defects (lower wavelengths) which are associated to the polycrystalline characteristics of films, while the epitaxial growth led to a lower energy emission (higher wavelengths) associated to the formation of shallow defects in the bandgap. To summarize, we have shown that the type of crystalline growth (polycrystalline or epitaxial), microstructure (dense or porous, shape and size of grains) and PL properties of the SST films can be tuned by changing composition, substrate type and deposition method.

Acknowledgements

Appendix A. Supplementary data

Supplementary data to this article can be found online at http://dx.doi.org/10.1016/j.surfcoat.2017.01.082.

References

[1] H.E. Swanson, R.K. Fuyat, G.M. Ugrinic, Powder diffraction file for perovskites strontium titanate, Nat. Bur. Stand. (US) Circ. 539 (1954) 44.
[2] P.C. Joshi, S.B. Krupanidhi, Structural and electrical characteristics of $SrTiO_3$ thin films for dynamic random access memory applications, J. Appl. Phys. 73 (1993) 7627–7634.
[3] J. Gallop, L. Hao, Single crystal microwave dielectrics at low temperature: losses and non-linearities, J. Eur. Ceram. Soc. 23 (2003) 2367–2373.
[4] T. Hara, T. Ishiguro, Oxygen sensitivity of $SrTiO_3$ thin film prepared using atomic layer deposition, Sens. Actuator. B-Chem. 136 (2009) 489–493.
[5] L.F. da Silva, W. Avansi Jr., J. Andrés, C. Ribeiro, M.L. Moreira, E. Longo, V. Mastelaro, Long-range and short-range structures of cube-like shape $SrTiO_3$ powders: microwave assisted hydrothermal synthesis and photocatalytic activity, Phys. Chem. Chem. Phys. 15 (2013) 12386–12393.
[6] A. Vegas, M. Vallet-Regí, J.M. González-Calbet, M.A. Alario-Franco, The $ASnO_3$ (A = Ca, Sr) perovskites, Acta Cryst B42 (1986) 167.
[7] A.-M. Azad, T.Y. Pang, M. Alim, Ultra-low temperature coefficient of capacitance (TCC) of the $SrSnO_3$-based electrical components, Act. Passive Electron. Compon. 26 (2003) 151–166.
[8] H. Wakana, S. Adachi, K. Tsubone, Y. Tarutani, A. Kamitani, K. Nakayama, Y. Ishimaru, K. Tanabe, Fabrication of high-temperature superconductor single-flux-quantum circuits using multilayer structure with a smooth surface, Supercond. Sci. Technol. 19 (2006) S312–S315.
[9] X. Hu, Y. Tang, T. Xiao, J. Jiang, Z. Jia, D. Li, B. Li, L. Luo, Rapid synthesis of single-crystalline $SrSn(OH)_6$ nanowires and the performance of $SrSnO_3$ nanorods used as anode materials for Li-ion battery, J. Phys. Chem. C 114 (2010) 947–952.

[10] C.W. Lee, D.W. Kim, I.S. Cho, S. Park, S.S. Shin, S.W. Seo, K.S. Hong, Simple synthesis and characterization of SrSnO₃ nanoparticles with enhanced photocatalytic activity, Int. J. Hydrog. Energy 37 (2012) 10557–10563.

[11] Y. Shimizu, M. Shimabukuro, H. Arai, T.J. Seiyama, Humidity sensitive characteristics of La³⁺-doped and undoped SrSnO₃, J. Electrochem. Soc. 136 (1989) 1206–1210.

[12] G.A. Smolenski, Physical phenomena in ferroelectrics with diffused phase transitions, J. Phys. Soc. Jpn. 28 (1970) 26–37.

[13] H.-H. Huang, M.-C Wang, C.-Y. Chen, N.-C. Wu, H.-J. Lin, Effect of deposition parameters on the growth rate and dielectric properties of the Ba(SnₓTi₁ ₋ ₓ)O₃ thin films prepared by radio frequency magnetron sputtering, J. Eur. Ceram. Soc. 26 (2006) 3211–3219.

[14] K.C. Singh, A.K. Nath, R. Laishram, O.P. Thakur, Structural, electrical and piezoelectric properties of nanocrystalline tin-substituted barium titanate ceramics, J. Alloys Compd. 509 (2011) 2597–2601.

[15] N. Horchidan, A.C. Ianculescu, L.P. Curecheriu, F. Tudorache, V. Musteata, S. Stoleriu, N. Dragan, C. Crisan, S. Tascu, L. Mitoseriu, Preparation and characterization of barium titanate stannate solid solutions, J. Alloys Compd. 509 (2011) 4731–4737.

[16] T. Shi, L. Xie, L. Gu, J. Zhu, Why Sn soping significantly enhances the dielectric properties of Ba(TᵢₓSn₁ ₋ ₓ)O₃, Sci. Rep. 5 (2015) 8606.

[17] W. Li, Z. Xu, R. Chu, P. Fu, G. Zang, Enhanced ferroelectric properties in (Ba₁ ₋ ₓCaₓ)(Ti₀.₉₄Sn₀.₀₆)O₃ lead-free ceramics, J. Eur. Ceram. Soc. 32 (2012) 517–520.

[18] J. Zhai, B. Shen, X. Yao, L. Zhang, Dielectric properties of Ba(SnₓTi₁ ₋ ₓ)O₃ thin films grown by a sol-gel process, Mater. Res. Bull. 39 (2004) 1599–1606.

[19] S. Song, J. Zhai, L. Gao, X. Yao, Orientation-dependent dielectric properties of Ba(Sn₀.₁₅Ti₀.₈₅)O₃ thin films prepared by sol-gel method, J. Phys. Chem. Solids 70 (2009) 1213–1217.

[20] G.H. Jain, L.A. Patil, V.B. Gaikwad, Studies on gas sensing performance of (Ba₀.₈Sr₀.₂)(Sn₀.₈Ti₀.₂)O₃ thick film resistors, Sensors Actuators B Chem. 122 (2007) 605–612.

[21] L. Wu, C.-C. Wu, M.-M. Wu, Humidity sensitivity of Sr(Sn,Ti)O₃ ceramics, J. Electron. Mater. 19 (1990) 197–200.

[22] A. Stanulis, A. Selskis, R. Ramanauskas, A. Beganskiene, A. Kareiva, Low temperature synthesis and characterization of strontium stannate-titanate ceramics, Mater. Chem. Phys. 130 (2011) 1246–1250.

[23] A.L.M. de Oliveira, M.R.S. Silva, H. Sales, E. Longo, A.S. Maia, A.G. Souza, I.M.G. dos Santos, Effect of the composition on the thermal behaviour of the SrSn₁ ₋ ₓTiₓO₃ precursor prepared by the polymeric precursor method, J. Therm. Anal. Calorim. 114 (2013) 565–572.

[24] K. Ueda, T. Maeda, K. Nakayashiki, K. Goto, Y. Nakachi, H. Takashima, K. Nomura, J. Kajihara, H. Hosono, Photoluminescence from epitaxial films of perovskite-type alkaline-earth stannates, Appl. Phys. Express 1 (2008) 015003.

[25] S. Lu, Z. Xu, Unusual strain dependence of tunability in highly (100)-oriented Mn-doped barium strontium stannate titanate thin films, Appl. Phys. Lett. 92 (2008) 232907.

[26] I.A. Souza, A.Z. Simões, S. Cava, L.S. Cavalcante, M. Cilense, E. Longo, J.A. Varela, Ferroelectric and dielectric properties of Ba₀.₅Sr₀.₅(Ti₀.₈₀Sn₀.₂₀O₃) thin films grown by the soft chemical method, J. Solid State Chem. 179 (2006) 2972–2976.

[27] Q. Liu, B. Li, H. Li, K. Dai, G. Zhu, W. Wang, Y. Zhang, G. Gao, J. Dai, Composition dependence of structural and optical properties in epitaxial Sr(Sn₁ ₋ ₓTiₓ)O₃ films, Jpn. J. Appl. Phys. 54 (2015) 031101.

[28] M.C.F. Alves, S. Boursicot, S. Ollivier, V. Bouquet, S. Députier, A. Perrin, I.T. Weber, A.G. Souza, I.M.G. Santos, M. Guilloux-Viry, Synthesis of SrSnO₃ thin films by pulsed laser deposition: influence of substrate and deposition temperature, Thin Solid Films 519 (2010) 614–618.

[29] M.C.F. Alves, R.M.M. Marinho, G.P. Casali, M. Siu-Li, S. Députier, M. Guilloux-Viry, A.G. Souza, E. Longo, I.T. Weber, I.M.G. Santos, V. Bouquet, Influence of the network modifier on the characteristics of MSnO₃ (M = Sr and Ca) thin films synthesized by chemical solution deposition, J. Solid State Chem. 199 (2013) 34–41.

[30] M.P. Pechini, Method of preparing lead and alkaline earth titanates and niobates and coating method using the same to form a capacitor, US Patent No. 3330697, July (1967).

[31] A. Vailionis, H. Boschker, W. Siemens, E.P. Houwman, D.H.A. Blank, G. Rijnders, G. Koster, Misfit strain accommodation in epitaxial ABO₃ perovskites: lattice rotations and lattice modulations, Phys. Rev. B 83 (2011) 064101.

[32] B.J. Kennedy, I. Qasim, K.S. Knight, Low temperature structural studies of SrSnO₃, J. Phys. Condens. Matter 27 (2015) 365401.

[33] A.S. Brown, M.A. Spackman, R.J. Hill, The electron distribution in corundum. A study of the utility of merging single-crystal and powder diffraction data, Acta Cryst A49 (1993) 513–527.

[34] H. Lehnert, H. Boysen, P. Dreier, Y. Yu, Room temperature structure of LaAlO₃, Z. Krist. 215 (2000) 145–147.

[35] R.D. Shannon, Revised effective ionic radii and systematic studies of interatomic distances in halides and chalcogenides, Acta Cryst A32 (1976) 751–767.

[36] C.Y. Fong, W. Weber, J.C. Phillips, Violation of Vegard's law in covalent semiconductor alloys, Phys. Rev. B 14 (1976) 5387–5391.

[37] P. Ganguly, N. Shah, M. Phadke, V. Ramaswamy, I.S. Mulla, Deviation from Vegard's law: changes in the c-axis parameter in La₂ ₋ ₓSrₓCuO₄ ₋ d in relation to the insulator-superconductor-metal transition, Phys. Rev. B 47 (1993) 991–995.

[38] F. Du, B. Cui, H. Cheng, R. Niu, Z. Chang, Synthesis, characterization, and dielectric properties of Ba(Ti₁ ₋ ₓSnₓ)O₃ nanopowders and ceramics, Mater. Res. Bull. 44 (2009) 1930–1934.

[39] E.R. Dobrovinskaya, L.A. Lytvynov, V. Pishchik, Sapphire: Material, Manufacturing, Applications, Springer Science, New York, 2009.

[40] P. Pandey, M. Sui, M.-Y. Li, Q. Zhang, E.-S. Kim, J. Lee, Shape transformation of self-assembled Au nanoparticles by the systematic control of deposition amount on sapphire (0001), RSC Adv. 5 (2015) 66212–66220.

[41] M. Zampieri, S.R. Lazaro, C.A. Paskocimas, A.G. Ferreira, E. Longo, J.A. Varela, Structural analysis of Ti and Pb citrate using NMR and FT-Raman signals and quantum mechanics simulations, J. Sol-Gel Sci. Technol. 37 (2006) 9–17.

[42] D. Bäuerle, Laser Processing and Chemistry, Springer, Heidleberg, Germany, 2011.

[43] M. Ohring, The Materials Science of Thin Films: Deposition and Structure, Academic Press, San Diego, USA, 2001.

[44] J.-H. Song, K.K. Kim, Y.J. Oh, H.-J. Jung, J.H. Song, D.-K. Choic, W.K. Choi, Twinned LaAlO₃ substrate effect on epitaxially grown La-Ca-Mn-O thin film crystalline structure, J. Cryst. Growth 223 (2001) 129–134.

[45] T. Yu, Y.-F. Chen, Z.G. Liu, N.-B. Min, X.-S. Wu, Epitaxial growth of dielectric SrTiO₃ thin films by pulsed laser deposition, Appl. Surf. Sci. 138 (1999) 605–608.

[46] M.R.S. Silva, M.C.F. Alves, V. Bouquet, S. Députier, G.P. Casali, I.T. Weber, S.M. Zanetti, E. Longo, M. Guilloux-Viry, A.G. Souza, I.M.G. Santos, Influence of Nd doping on the properties of SrTiO₃ thin films synthesized by PLD on different substrates, Curr. Phys. Chem. 3 (2013) 392–399.

[47] L.F. da Silva, L.J.Q. Maia, M.I.B. Bernardi, J.A. Andrés, V.R. Mastelaro, An improved method for preparation of SrTiO₃ nanoparticles, Mater. Chem. Phys. 125 (2011) 168.

[48] V.M. Longo, A.T. de Figueiredo, S. de Lázaro, M.F. Gurgel, M.G.S. Costa, C.O. Paiva-Santos, J.A. Varela, E. Longo, V.R. Mastelaro, F.S. de Vicente, A.C. Hernandes, R.W.A. Franco, Structural conditions that leads to photoluminescence emission in SrTiO₃: an experimental and theoretical approach, J. Appl. Phys. 104 (2008) 023511.

[49] V.L. Longo, L.S. Cavalcante, M.G.S. Costa, M.L. Moreira, A.T. de Figueiredo, J. Andrés, J.A. Varela, E. Longo, First principles calculations on the origin of violet-blue and green light photoluminescence emission in SrZrO₃ and SrTiO₃ perovskites, Theor. Chem. Accounts 124 (2009) 385.